Acta Oceanol. Sin., 2018, Vol. 37, No. 3, P. 73–79
DOI: 10.1007/s13131-017-0986-2
http://www.hyxb.org.cn
E-mail: hyxbe@263.net

The deep structure of the Duanqiao hydrothermal field at the Southwest Indian Ridge

SUN Chaofeng[1, 2], WU Zhaocai[1, 2], TAO Chunhui[1, 2*], RUAN Aiguo[1, 2], ZHANG Guoyin[1, 2], GUO Zhikui[1, 2, 3], HUANG Enxian[4]

[1] Key Laboratory of Submarine Geosciences, State Oceanic Administration, Hangzhou 310012, China

[2] Second Institute of Oceanography, State Oceanic Administration, Hangzhou 310012, China

[3] Institute of Geophysics and Geomatics, China University of Oceanography, Wuhan 430074, China

[4] Henan Province Earthquake Administration, Zhengzhou 450016, China

Received 24 April 2016; accepted 25 May 2016

Abstract

Polymetalic sulfide is the main product of sea-floor hydrothermal venting, and has become an important sea-floor mineral resources for its rich in many kinds of precious metal elements. Since 2007, a number of investigations have been carried out by the China Ocean Mineral Resources Research and Development Association (COMRA) cruises (CCCs) along the Southwest Indian Ridge (SWIR). In 2011, the COMRA signed an exploration contract of sea-floor polymetallic sulfides of 10 000 km^2 on the SWIR with the International Seabed Authority. Based on the multibeam data and shipborne gravity data obtained in 2010 by the R/V *Dayang Yihao* during the leg 6 of CCCs 21, together with the global satellite surveys, the characteristics of gravity anomalies are analyzed in the Duanqiao hydrothermal field (37°39′S, 50°24′E). The "subarea calibration" terrain-correcting method is employed to calculate the Bouguer gravity anomaly, and the ocean bottom seismometer (OBS) profile is used to constrain the two-dimensional gravity anomaly simulation. The absent Moho in a previous seismic model is also calculated. The results show that the crustal thickness varies between 3 and 10 km along the profile, and the maximum crustal thickness reaches up to 10 km in the Duanqiao hydrothermal field with an average of 7.5 km. It is by far the most thicker crust discovered along the SWIR. The calculated crust thickness at the Longqi hydrothermal field is approximately 3 km, 1 km less than that indicated by seismic models, possibly due to the outcome of an oceanic core complex (OCC).

Key words: crustal thickness, Duanqiao hydrothermal field, gravity anomaly, polymetallic sulfides, Southwest Indian Ridge

Citation: Sun Chaofeng, Wu Zhaocai, Tao Chunhui, Ruan Aiguo, Zhang Guoyin, Guo Zhikui, Huang Enxian. 2018. The deep structure of the Duanqiao hydrothermal field at the Southwest Indian Ridge. Acta Oceanologica Sinica, 37(3): 73–79, doi: 10.1007/s13131-017-0986-2

1 Introduction

A new oceanic crust is generated at the mid-ocean ridge (MOR) by decompression melting, upwelling and cooling of the underlying mantle (Plank and Langmuir, 1992; Asimow and Langmuir, 2003). The spreading process is accompanied by volcanic, seismic and hydrothermal activities. Hydrothermal venting occurred along MOR is a thermodynamic process of interaction among magmatism, tectonism (Tucholke et al., 1998; Okino et al., 2004; Escartín et al., 2008) and biogeochemistry (Lowell, 2008; Liu et al., 2011). The polymetallic sulfides, enriched in precious metal elements such as copper, zinc, plumbum, gold, and argentum, are commonly associated with active hydrothermal vents near or at a mid-ocean ridge, island-arcs and back-arc basins (Baker and German, 2004), and are considered as another ocean resources with broad prospects for the development besides the polymetallic nodules and cobalt-rich crust (Galley, 1993; Ding et al., 2009).

Most MORs in a seabed area are located far away from continent with complicated geological structure (Alt, 2003; Stein and Stein, 1994; Tivey, 2007; Martin et al., 2008; German and Lin, 2004). Relative to thousands of meters of the depth, it is difficult to determine the geophysical characteristics of the decameter-scale hydrothermal sulfide vents (Tivey and Dyment, 2010), therefore most of the researches mainly focus on the activity and origin of hydrothermal vent systems (Yao et al., 2011; Tao et al., 2012).

From 2005 to 2015, the China Ocean Mineral Resources Research and Development Association organized eight cruises, including 23 legs, to investigate sea-floor hydrothermal activity. In 2007, during the 19th CCC, the first active hydrothermal vent (the Longqi) (Tao et al., 2012) was discovered at 49.6°E of the ultralslow spreading SWIR. During 2008–2009, the R/V *Dayang Yihao* detected other hydrothermal fields at 49°–52°E by the presence of a turbidity anomaly including the Duanqiao (Tao et al. 2009, 2012). The presence of these hydrothermal fields dis-

Foundation item: The National Basic Research Program (973 Program) of China under contract No. 2012CB417305; the China Ocean Mineral Resources Research and Development Association Twelfth Five-Year Major Program under contract Nos DY125-11-R-01 and DY125-11-R-05; the International Cooperative Study on Hydrothermal System at Ultraslow Spreading SWIR; the Natural Science Foundation of Zhejiang Province of China under contract No. LY12D06006; the Scientific Research Fund of Second Institute of Oceanography, State Oceanic Administration under contract No. JG1203.
*Corresponding author, E-mail: taochunhuimail@163.com

covered along the SWIR, however, is not very consistent with the proposed relation between the MOR spreading rates and the associated hydrothermal activity (Baker et al., 1996). Tao et al. (2012) hypothesize that local magma supply and crustal permeability play primary roles in controlling the distribution of hydrothermal activities. On the basis of the multi-beam data and shipborne gravity data obtained by the R/V *Dayang Yihao*, combined with the multibeam data and OBS data, we studied the deep structure of the Duanqiao hydrothermal field.

2 Regional geological setting

The ultra-slow spreading ridges, principally include the Southwest Indian Ridge and the Gakkel Ridge, are the ridges with full spreading rates less than 20 mm/a, which make up 25% of the global ridge length (Edmonds et al., 2003). The SWIR extends westward from the Rodriguez triple junction (RTJ) to the Bouvier triple junction (BTJ). The total length of the SWIR is approximately 7 700 km with a spreading rate varying from 14 to 16 mm/a (Dick et al., 2003; Tao et al., 2014). The spreading rate of the west segment is slightly higher than the east segment (Dick et al., 2003; Cannat et al., 2004), yet the variation along the axial direction is not apparent (Sauter and Cannat, 2010). The geological and geophysical characteristics of the SWIR, such as the water depth of the ridge axis, geomorphologic characteristics, crustal depth, underlying mantle composition (Meyzen et al., 2003; Seyler et al., 2003), magmatism (Font et al., 2007; Sauter et al., 2001; Georgen et al., 2003), etc. present significant variations from the BTJ to the RTJ. Therefore, the SWIR is divided into several ridge segments according their geometry and extensional history. The sea-floor topography in the SWIR records alternate regions of uplift and depression and the development of axial rifts. The SWIR is highly segmented by NNE-trend faults (Dick et al., 2000). The topographic variation, distribution of boundary faults, geometric shape and extensional history allow the SWIR to be subdivided into seven segments form west to east (Fisher and Goodwillie, 1997; Georgen et al., 2001). Four ridge segments are limited by the Discovery, Gallieni and Melville facture zone, respectively (Mendel et al., 2003). Seismic data reveals that different segments crustal structure is parallel along the ridge axis with an average thickness of 5 km. The segments are characterized by concentrated magma, thick crust at the spreading segment and thin crust in non-transform discontinuous (NTD) or mid-ridge rifts (Niu et al., 2015; Li et al., 2015a, b). The gravity data indicate substantial topographic variations along the SWIR axis except the zones affected by transform faults. The depth of the SWIR gradually increases and residual mantle Bouguer anomaly (RMBA) values increase progressively from west to east with a gradual diminution in crustal thickness (Sauter et al., 2001; Suo, 2014). A similar fluctuation occurs of the mantle Bouguer anomaly (MBA) and RMBA in medium or in large-scale along the SWIR axial direction (Georgen et al., 2001), which indicates that the SWIR is rarely affected by thermal at the medium or large scale.

The Duanqiao hydrothermal field is located at an axial highland with shallow sea-water (≈1 700 m) and the surrounding terrane is relatively flat (Tao et al., 2014). The Duanqiao hydrothermal field is one of the shallowest area of the entire SWIR and corresponds to a mantle Bouguer anomaly indicating the presence of a thick crust or low density body. Ruan et al. (2014) show that the Duanqiao hydrothermal field, as an inactive hydrothermal field, has the maximum crustal thickness up to 10.8 km, and probably a magma chamber within the lower crust. The fact that the Duanqiao hydrothermal field occurs over a past or present magma chamber is consistent with the magma budget hypothesis (Baker et al., 1996). On the basis of the small-scale depth variations of the ridge axis, Cannat et al. (1999) divided the 49°–69°E of SWIR into 26 ridge segments and placed the Duanqiao into Segment 27. The depth of the axial ridge varies between 1 500 and 3 500 m and it is the shallowest zone of 49°–69°E segment. Compared with the average depth of other ridge axis and volcanic centers of other segments of the SWIR, it indicates an important supply of magma in the Duanqiao hydrothermal field(Sauter et al., 2009; Li et al., 2015a, b). A large number of silica-rich sediments (opal) and sulfide samples were collected from the Duanqiao hydrothermal field, with a smaller number of tabular anhydrite and framboidal pyrite samples also gathered (Tao et al., 2009). However, so far we have not detected any temperature or turbidity anomalies, the Duanqiao hydrothermal field is probably inactive (Tao et al., 2014).

3 Data and method

3.1 *Data*

The gravity data and bathymetry were mainly obtained from ship-borne gravity and multi-beam seaf-loor topography surveys during the Leg 6 of CCC 21, at the Duanqiao hydrothermal field (Fig. 1). A S-129 type ocean gravimeter is employed to measure gravity, its accuracy is ±1 mGal, and its static sensitivity is 0.01 mGal with the range of 12 000 mGal (global range), the linear drift was <3.0 mGal/month, and the maximum operating angle of its gyro-stabilized platform is ±25°. The localization signal matching the gravity observation is the from Ominstar differential GPS signal with accuracy of ±10 m or less taken with the GMT. The selected gravity survey line is conformed to the measurement standards by comparing the measured ship's course and speed change. The mean square root is used to estimate the intersection of free air gravity anomaly (FAA) of each survey line (2.743 mGal). The measurements meet the requirements of National Oceanographic Survey Code (GB/T 12763.8-2007) gravity surveys scale of 1:500 000 or less and the mean square root of free air anomaly being <3 mGal.

3.2 *Method*

The free air gravity anomaly and Bouguer gravity anomaly are obtained through data processing, such as dividing and summarizing the survey lines, calibrating the time and location and applying the normal field, free air and Bouguer corrections.

3.2.1 *Time constant correction*

Ocean gravity surveys were conducted under harsh conditions. To obtain high precision measurements, a strong damping device is set in the probe to cut interferences in addition to installing a gravimeter (probe) above gyro platforms. The filtering processing is performed via software. The gravity instrument generates a lag-time effect so that the data recorded at one moment is actually the gravity value obtained several minutes ago at another position. When an ocean survey is performed, the lag-time of the S-129 type gravimeter is 6 min; the date recorded by gravimeter at some moment may correspond to its position before 6 min. When the gravity data from the base points located on a pier are compared before and after the measurements, the difference in the base point gravity values is distributed in pro rata to the read values of the gravimeter.

3.2.2 *Eotvos correction*

S-II ocean gravimeters use a built-in filter to conduct low-pass filtering through the exact Blackman window function,

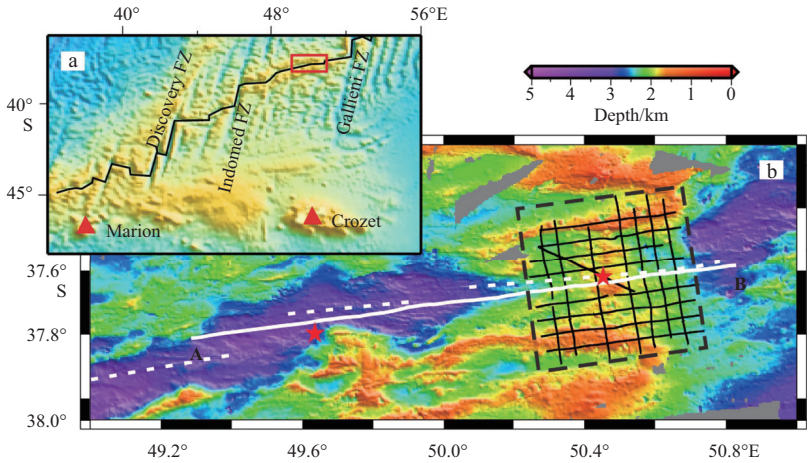

Fig. 1. Map of survey lines. The black and white solid lines represent all surveyed lines, the white survey lines are gravity profiles chosen for analyses, white dashed lines depict the ridge axis, the black dashed area represents the Duanqiao hydrothermal field and the red stars show the hydrothermal fields.

which advantages include a linear phase frequency and a data fidelity. Nevertheless, there is a lag in the recording time of data. The default lagging time is usually 361 s, namely each 180 s of the gravity data before and after this measured point is filtered. The filtering reflects the gravity value obtained before and after 180 s, causing a 180 s lag (LaCoste and Romberg Company, 2004; Zhang et al., 2005). Therefore, this lag time must be eliminated when the Eotvos correction is applied through the same filtering process. The time domain of the S-II ocean gravimeter built-in filter and the feature of frequency domain calculated by a mathematic formula in the exact Blackman window function are combined to design a similar low-pass filter.

3.2.3 *Calculation of the Bouguer gravity anomaly*

We subtract the topographical effect on the gravity survey to obtain the Bouguer gravity anomaly (BGA) to reflect the density variations according to the water depth. Since the multibeam detects a 100 m×100 m grid on the sea-floor with precision and the ETOPO1 only analyze a 2 km×2 km grid, we adopted a specific topographic partition arrangement. The area for a topographic correction is subdivided into three zones: near, junction and far zones, respectively. In the near zone, the range of the topographic corrections, calculated by the right prism formula with grid of 100 m×100 m, is 0–2 000 m. In the far zone, the range of topographic corrections is 2–166.7 km. The far zone is then subdivided into seven circular zones with radius of 2–20, 20–44, 44–68, 68–92, 92–116, 116–140 and 140–166.7 km, respectively. Each ring zone is uniformly subdivided into 16 bands and a spherical coordinate method is used to calculate the topographic correction. Within the junction zone located between the square-shape near zone and the circle-shape far zone, a supplementary angle formula was employed to calculate the topographic correction. In all calculations, we used a seawater density 1.03 g/cm^3 and oceanic crustal density 2.7 g/cm^3 (General Administration of Quality Supervision, Inspection and Quarantine of the People's Republic of China, and Standardization Administration of the People's Republic of China, 2007).

4 Results and discussion

4.1 *Free air and Bouguer gravity anomalies*

The free air gravity anomaly of the Duanqiao hydrothermal field is constrained between –30×10^{-5} and 18×10^{-5} m/s^2 (Fig. 2). The anomaly presents a ridge-like shape with low values at the east and west extremities and relatively high values in the middle area, and no significant variations correlated with the width of the ridge. The space anomaly mainly reflects different elevations and changes in the density of the oceanic lithosphere, and the first-order approximation of the topography.

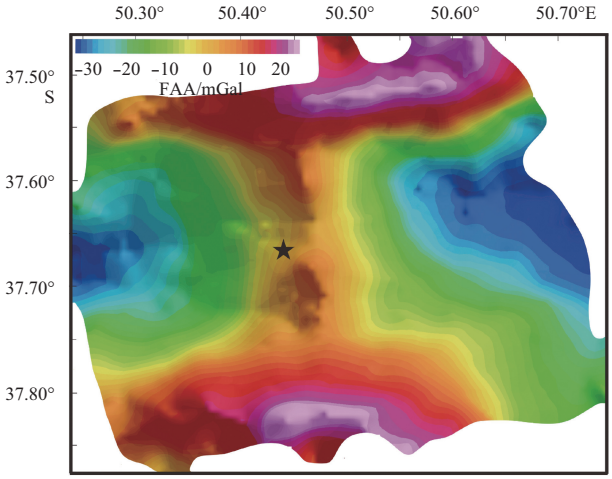

Fig. 2. Map of the free air gravity anomaly corresponding to the Duanqiao hydrothermal field.

The ship-borne multi beam data and global the ETOPO1 water depth data are combined with the calculated the Bouguer gravity anomaly subtracting the effect of water depth (topography). Figure 3 reveals that the Bouguer gravity anomaly mimics the shape of the Moho. The results show that the Bouguer gravity anomaly varies from 100×10^{-5} to 165×10^{-5} m/s^2 forming a trough shape (two high limbs and a low middle). The comparison of Fig. 2 and Fig. 3 shows that the free air gravity anomaly is relatively high, whereas the Bouguer gravity anomaly is relatively low. Therefore, we infer that the oceanic crust is thick in this area.

4.2 *Combining the gravity-seismic inversion of typical profiles*

A survey line along the ridge axis is selected to be analyzed in detail. The EW-oriented and 120 km long line starts from 37.81°S,

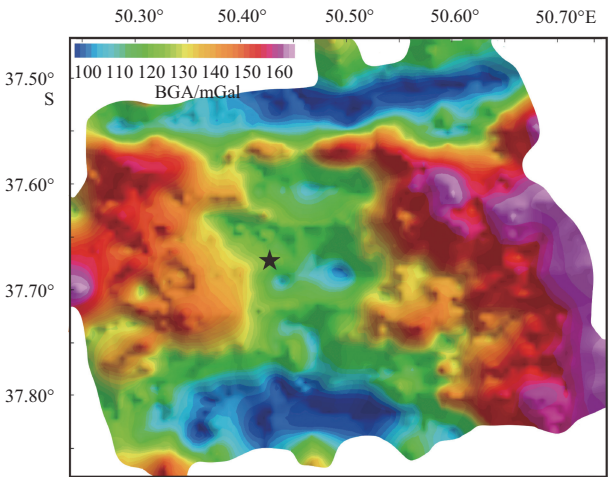

Fig. 3. Map of the Bouguer gravity anomaly corresponding to the Duanqiao hydrothermal field.

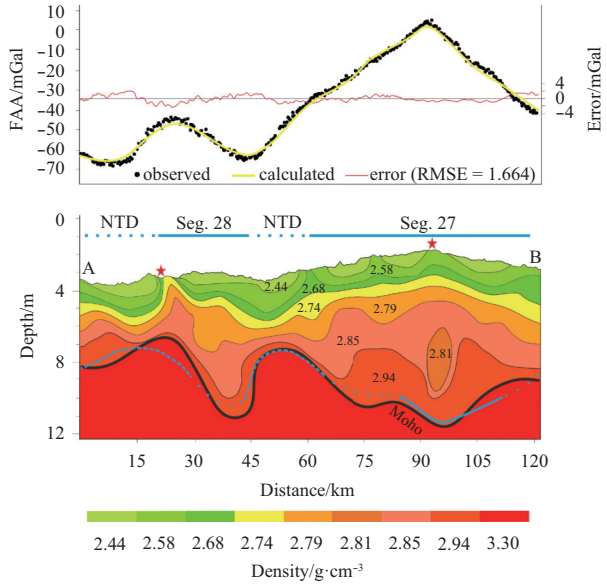

Fig. 4. Density profile. The black solid line is the stratified interface of the density profile, the black heavy solid line is the Moho got by inverting gravity data, the blue solid line is Moho extracted from a 3-D seismic tomography model, the blue dashed line is Moho inferred from the mantle velocity, the blue dotted line is Moho calculated by interpolation (Li et al., 2015a, b), and the red stars are the location of the hydrothermal fields.

49.29°E, and ends at 37.64°S, 50.83°E. The variations of free air anomaly amplitudes are between -73.65×10^{-5} and 7.85×10^{-5} m/s^2 and the anomaly displays a wave-peak shape with the maximum value at 37.68°S and 50.47°E, coincident with topographic fluctuations. The Bouguer gravity anomaly reflects the undulated boundary between the oceanic crust and mantle and also various geologic bodies with different densities from that of the oceanic crust. Locally, areas with low Bouguer gravity anomaly values indicate a thicker oceanic crust relative to those of a "normal" or low density crust, whereas the high value areas possess a thinner crust relative to those of a "normal" crust or high density crust. The variations of the Bouguer gravity anomaly values on the survey line change from 114.01×10^{-5} to 190.43×10^{-5} m/s^2 and the anomaly display a trough shape. In which the maximum free air gravity anomaly corresponds to the minimum Bouguer gravity anomaly.

We also simulated the gravity data to study the crustal density structure of the Duanqiao hydrothermal field along the direction of the oceanic ridge (Fig. 4), referred to previous research at Duanqiao hydrothermal field in the SWIR (Zhang et al., 2013; Ruan et al., 2014; Niu et al., 2015; Li et al., 2015a, b) and the oceanic crust model proposed by Vine and Moores (1972) and Minshull et al. (2006). On the basis of the measured gravity data (Tao et al., 2013), we modified the empirical formula of the relation between the Gardner et al. (1974) density law and the seismic P-wave to be $\rho=0.315V^{0.25}$. The initial density model of the oceanic crust profile is established through the velocity profile inverted from the OBS data (Li et al., 2015a, b). The seawater density is set at 1.03 g/cm^3 and that of the mantle at 3.30 g/cm^3.

The comparison of the Moho calculated using the gravity anomalies with that obtained by the seismic profiles shows a comparable morphology and depth. The Moho inverted from the gravity data below the Duanqiao hydrothermal field (85–110 km) tightly coincides with the Moho calculated from the PmP seismic profiles using a tomographic method (Li et al., 2015a, b). Therefore, the Moho, calculated by the gravity inversion is relatively accurate. However, in the part of the blue dotted line (30–45 and 65–80 km), the Moho calculated by interpolation shows a large discrepancy, the gravity Moho 1 km deeper than the seismic Moho. Moreover, the location of the Longqi hydrothermal field is 15–30 km away from Point A (Fig. 4), so that the depth of the Moho converted from the gravity is 1 km shallower than that of the seismic inversion. This may be due to the relatively thin oceanic core complex (OCC) near the Longqi hydrothermal field (Zhao et al., 2013), which influences the results of the gravity inversion.

The oceanic crust thickness varies along mid-ridge. The crust is thick at the center of the oceanic ridge, while it is thin at the extremities or at non-transform discontinuous segments (NTD). From the map profiles, there is a clear variation in crustal thickness, between 3 and 10 km, along the MOR. The crustal thickness of the Longqi hydrothermal field, located at the west end of the 28th oceanic segment, is thinner (≈3 km), whereas the crust of the Duanqiao hydrothermal field, which lies at the center of 27th oceanic segment, is generally thicker with an average thickness of 7.5 km. The thickest crust situated below the hydrothermal field is 10 km. This is not consistent with the proposed relation between the global spreading rate and the crustal thickness (Chen, 1992). Nevertheless, our results conform to the range of the crustal thickness inverted by Mendel et al. (2003) using the gravity data and are also close to the seismic results (Ruan et al., 2014; Li et al., 2015a, b).

On the basis of the seismic results of Li et al. (2015b), our research improves the knowledge of the crustal thickness beneath Duanqiao field and adds to the morphologic variation of the Moho which cannot be known by seismic data. The seismic and gravity data allow a finer definition of the deep crustal structure. The seismic profile displays a low velocity body (Li et al., 2015a, b) which corresponds to the low density body depicted in Fig. 4. This suggests that the low density body constitutes a magma chamber supplying a vast amount of heat into the oceanic ridge; a prerequisite to the formation of sea-floor polymetallic sulfides along with a crustal fracturation.

In the very slow spreading MOR, magmatic and amagmatic extensions coexist (Dick et al., 2003, but the magmatism is dominant at magmatic extensional center (Li et al., 2015a, b). Sporad-

ic magmatism is concentrated in certain spots along the very slow spreading mid-oceanic ridge, and the overall magmatic supply is insufficient (Cannat et al., 1999; Sauter et al., 2001; Standish et al., 2008). The formation of thick crust may depend on focusing a high volume of magma at the center of the segment. However, Georgen et al. (2001) and Sauter et al. (2009) speculated the thickening of the crust or the increase in mantle temperature in Duanqiao was related to the upwelling of the Crozet hotspot which is located 1 000 km southward; Zhou and Dick (2013) argued that, rather than crustal thickening, an early melting event leaving a low density depleted mantle occurred under the SWIR. On the contrary, Li et al. (2015b) hold the opinion there is a large amount of magma associated with the heterogeneous mantle characterized by high temperature and a very efficient focusing mechanism of melt delivery.

Hotspots such as Marion, Crozet and others can change the morphology, mantle composition flow and thermal structure under mid-oceanic ridges. They can further alter the growth of oceanic crust, affect the hydrothermal mineralization and structural characteristics, especially of very slow spreading mid-oceanic ridges (Dick et al., 2003; Cannat et al., 2006; Standish and Sims, 2010; Li et al., 2015a, b). The study shows the effect of the Marion hotspot being restricted by large transform fault because they can divide and even hinder the magma flow at mid-ocean ridges (Ribe et al., 1995; Ribe, 1996; Ito et al., 1997, 1999; Georgen et al., 2003). The effect is significant when the magma flow abuts the Discovery II transform fault (Zhang et al., 2011). Therefore, in the study area, the supply of magma may comes from the Crozet hotspot (Georgen et al., 2001; Sauter et al., 2009; Zhang et al., 2013). The location of the 10 km-thick segment (50.24°E) is adjacent and lies on the west of the Gallieni transform fault. There is a huge difference in crustal thickness between the two sides of the Gallieni transform fault. Therefore, it is possible the transform, which displays a large displacement, may impede the migration of magma, creating an excess of magma on one side of the transform fault. The formation of thick oceanic crust below the Duanqiao field may be caused by the migration of the Crozet hotspot toward the SWIR (Zhang et al., 2011), with the Gallieni transform fa.ult preventing the migration of melt flow. Consequently, a thick crust was built on the west side of the Gallieni transform fault (50.24°E). When a large magmatic center is covered by thin a lithosphere at a very slow spreading MOR, the surrounding magma overlain by a thick lithosphere will converge toward the asthenosphere under the magmatic center (Li et al., 2015a, b). Therefore, a combination of factors such the mantle heterogeneity (high temperature and sufficient magmatic source), a very efficient melting mechanism (Li et al., 2015a, b), the presence of the Crozet hotspot and the Gallieni transform fault (Georgen et al., 2001; Sauter et al., 2009; Zhang et al., 2013; Ruan et al., 2014) will generate an anomalous amount of magma below the hydrothermal vent.

Seafloor hydrothermal polymetallic sulfides are generated by water-rock hydrothermal interaction in the oceanic crust. Hydrothermal circulation is a basic process controlling the transport of energy and elements from the lithosphere to the hydrosphere (Nath, 2007). The principal factors governing the seafloor hydrothermal sulfide mineralization are magmatism and deep crustal fracturing (Charlou et al., 1996). The gravity profile map reveals the Duanqiao hydrothermal field is located on the west side of Gallieni transform fault, so that hydrothermal fluids percolate upward along faults to build a dome of sulfide. The topography, gravity and seismic data indicate the thick crust diverges from the ridge axis and extends for at least 20 km along the spreading direction of the oceanic ridge. This suggests an increase in mantle melting lasting at least 3 Ma or even 10 Ma (Sauter et al., 2009; Li et al., 2015a, b). Such a long-term and stable supply of magma generates intense sea-floor hydrothermal activity producing ample material for sul-fide accumulation near the Duanqiao. Since the gravity survey is conducted at sea, the gravity anomaly associated with sulfide mineralization is only parts per million of metre per second squared. Therefore, to delineate the scope of sulfide mineralization and calculate the tonnage of an orebody, it is necessary to improve data accuracy and to carry out more sea-floor gravity surveys.

5 Conclusions

The geology of the SWIR is especially complex with variable geological-geophysical signatures and numerous sea-floor hydrothermal vents. The Duanqiao hydrothermal site is associated with the formation of polymetallic sulfides. We have studied the gravity anomalies to understand its deep geological structure and reveal the potential of the sulfide mineral resources.

We eliminate the effect of the surrounding topography, which improves the accuracy of terrain correction. The subarea topography calibration method, commonly used in onshore gravity prospecting, serves to correct the ship-borne gravity data. The gravity simulation process leads to the following conclusions.

(1) The depth of Moho, which cannot be inverted due to the missing seismic data, is simulated by the gravity data and the deep fine geological structure is obtained.

(2) As a result, we found that an imbalance in the crustal thickness is observed along the direction of the mid-ocean ridge. The crust is thick at the center of the oceanic ridge segment, while it is thin at the extremities or at non-transform discontinuous belts (NTD). The SWIR is one of the earth's slowest spreading mid-oceanic ridge, having a crustal thickness of 3 and 10 km along the surveying line. The oceanic crust in the Longqi hydrothermal field, located at the western end of the 28th segment, is thinner ≈3 km). This may be related to the effect of a nearby oceanic core complex (OCC), whereas the crust below the non-active Duanqiao hydrothermal field, sitting in the middle of the 27th oceanic segment, is nearly 10 km thickness. The average thickness of the surrounding crust is 7.5 km. Therefore, the crustal structure does not conform to the relation between the global spreading rate and crustal thickness.

(3) We speculate that the Duanqiao hydrothermal field is an aresource prospect area for polymetallic sulfides owing to the role of the Gallieni transform fault and long-term and stable supply of magma.

Acknowledgements

The authors thank the captains, crew and the science parties who participated the DY115-21 cruises on R/V *Dayang Yihao*. We also thank Edward T Baker and Liang Jin for helpful comments on this paper.

References

Alt J C. 2003. Hydrothermal fluxes at mid-ocean ridges and on ridge flanks. Comptes Rendus Geoscience, 335(10-11): 853–864

Asimow P D, Langmuir C H. 2003. The importance of water to oceanic mantle melting regimes. Nature, 421(6925): 815–820

Baker E T, Chen Y J, Jason P M. 1996. The relationship between near-axis hydrothermal cooling and the spreading rate of mid-ocean ridges. Earth and Planetary Science Letters, 142(1-2): 137–145

Baker E T, German C R. 2004. On the global distribution of hydrothermal vent fields. In: German C R, Lin Jian, Parson L M, et al., eds. Mid-Ocean Ridges: Hydrothermal Interactions Between

the Lithosphere and Oceans. Washington DC: American Geophysical Union, 245–266
Cannat M, Rommevaux-Jestin C, Sauter D, et al. 1999. Formation of the axial relief at the very slow spreading Southwest Indian Ridge (49° to 69°E). Journal of Geophysical Research, 104(B10): 22825–22843
Cannat M, Sauter D, Mendel V, et al. 2004. Spreading geometry and melt supply at the ultraslow-spreading Southwest Indian Ridge. In: AGU Fall Meeting Abstracts 2004. v 1. Washington DC : American Geophysical Union, 3
Cannat M, Sauter D, Mendel V, et al. 2006. Modes of seafloor generation at a melt-poor ultraslow-spreading ridge. Geology, 34(7): 605–608
Charlou J L, Fouquet Y, Donval J P, et al. 1996. Mineral and gas chemistry of hydrothermal fluids on an ultrafast spreading ridge: east Pacific Rise, 17° to 19°S (Naudur cruise, 1993) phase separation processes controlled by volcanic and tectonic activity. Journal of Geophysical Research, 101(B7): 15899–15919
Chen Y J. 1992. Oceanic crustal thickness versus spreading rate. Geophysical Research Letters, 19(8): 753–756
Dick H J B, Lin Jian, Schouten H. 2003. An ultraslow-spreading class of ocean ridge. Nature, 426(6956): 405–412
Dick H J B, Natland J H, Alt J C, et al. 2000. A long in situ section of the lower ocean crust: results of ODP leg 176 drilling at the Southwest Indian Ridge. Earth and Planetary Science Letters, 179(1): 31–51
Ding Liuhuai, Chen Ximing, Gao Yuqing. 2009. Seafloor massive sulfides: the frontier of deep ocean miming. Ocean Technology (in Chinese), 28(1): 126–132
Edmonds H N, Michael P J, Baker E T, et al. 2003. Discovery of abundant hydrothermal venting on the ultraslow-spreading Gakkel Ridge in the Arctic Ocean. Nature, 421(6920): 252–256
Escartín J, Smith D K, Cann J, et al. 2008. Central role of detachment faults in accretion of slow-spreading oceanic lithosphere. Nature, 455(7214): 790–794
Fisher R L, Goodwillie A M. 1997. The physiography of the Southwest Indian Ridge. Marine Geophysical Researches, 19(6): 451–455
Font L, Murton B J, Roberts S, et al. 2007. Variations in melt productivity and melting conditions along SWIR (70°–49°E): evidence from olivine-hosted and plagioclase-hosted melt inclusions. Journal of Petrology, 48(8): 1471–1494
Galley A G. 1993. Characteristics of semi-conformable alteration zones associated with volcanogenic massive sulphide districts. Journal of Geochemical Exploration, 48(2): 175–200
Gardner G H F, Gardner L W, Gregory A R. 1974. Formation velocity and density-the diagnostic basics for stratigraphic traps. Geophysics, 39(6): 770–780
General Administration of Quality Supervision, Inspection and Quarantine of the People's Republic of China, Standardization Administration of the People's Republic of China. 2007. GB /T 12763.8-2007 Specifications for Oceanographic Survey. Beijing: Standards Press of China
Georgen J E, Kurz M D, Dick H J B, et al. 2003. Low $^{3}He/^{4}He$ ratios in basalt glasses from the western Southwest Indian Ridge (10°–24°E). Earth and Planetary Science Letters, 206(3–4): 509–528
Georgen J E, Lin Jian. 2003. Plume-transform interactions at ultraslow spreading ridges: implications for the Southwest Indian Ridge. Geochemistry, Geophysics, Geosystems, 4(9): 9106
Georgen J E, Lin Jian, Dick H J B. 2001. Evidence from gravity anomalies for interactions of the Marion and Bouvet hotspots with the Southwest Indian Ridge: effects of transform offsets. Earth &Planetary Science Letters, 187(3): 283–300
German C R, Lin Jian. 2004. The thermal structure of the oceanic crust, ridge-spreading and hydrothermal circulation: How well do we understand their Inter-Connections. In: German C R, Lin Jian, Parson L M, eds. Mid-Ocean Ridges: Hydrothermal Interactions Between the Lithosphere and Oceans. Washington DC: American Geophysical Union, 1–18
Ito G, Lin Jian, Gable C W. 1997. Interaction of mantle plumes and migrating mid-ocean ridges: implications for the Galápagos plume-ridge system. Journal of Geophysical Research, 102(B7): 15403–15417
Ito G, Shen Yang, Hirth G, et al. 1999. Mantle flow, melting, and dehydration of the Iceland mantle plume. Earth and Planetary Science Letters, 165(1): 81–96
LaCoste and Romberg Company. 2004. Model "S" Air-Sea Dynamic Gravity Meter System II Instruction Manual. Austin: LaCoste and Romberg Company
Li Jiabiao, Jian Hanchao, Chen Y J, et al. 2015a. Seismic observation of an extremely magmatic accretion at the ultraslow spreading Southwest Indian Ridge. Geophysical Research Letters, 42(8): 2656–2663
Li Sanzhong, Suo Yanhui, Liu Xin, et al. 2015b. Tectonic reconstruction and mineralization models of the Indian Ocean: insights from SWIR. Geotectonica et Metallogenia (in Chinese), 39(1): 30–43
Liu Weiyong, Zheng Lianfu, Tao Chunhui, et al. 2011. On the feature of seafloor hydrothermal systems' evolutionary and its mineralization in Mid-Ocean Ridge. Journal of Marine Sciences (in Chinese), 29(1): 25–33
Lowell B. 2008. Focus on Modeling: state of the art & future challenges. Ridge 2000 Events (summer), 5–9
Martin W, Baross J, Kelley D, et al. 2008. Hydrothermal vents and the origin of life. Nature Reviews Microbiology, 6(11): 805–814
Mendel V, Sauter D, Rommevaux-Jestin C, et al. 2003. Magmato-tectonic cyclicity at the ultra-slow spreading Southwest Indian Ridge: evidence from variations of axial volcanic ridge morphology and abyssal hills pattern. Geochemistry, Geophysics, Geosystems, 4(5): 9102
Meyzen C M, Toplis M J, Humler E, et al. 2003. A discontinuity in mantle composition beneath the Southwest Indian Ridge. Nature, 421(6924): 731–733
Minshull T A, Muller M R, White R S. 2006. Crustal structure of the Southwest Indian Ridge at 66°E: seismic constraints. Geophysical Journal International, 166(1): 135–147
Nath B N. 2007. Hydrothermal Minerals. Indian: National institute of Oceanography, 78–83
Niu Xiongwei, Ruan Aiguo, Li Jiabiao, et al. 2015. Along-axis variation in crustal thickness at the ultraslow spreading Southwest Indian Ridge (50°E) from a wide-angle seismic experiment. Geochemistry, Geophysics, Geosystems, 16(2): 468–485
Okino K, Matsuda K, Christie D M, et al. 2004. Development of oceanic detachment and asymmetric spreading at the Australian-Antarctic discordance. Geochemistry, Geophysics, Geosystems, 5(12): Q12012
Plank T, Langmuir C H. 1992. Effects of the melting regime on the composition of the oceanic crust. Journal of Geophysical Research, 97(B13): 19749–19770
Ribe N M. 1996. The dynamics of plume-ridge interaction: 2. Off-ridge plumes. Journal of Geophysical Research, 101(B7): 16195–16204
Ribe N M, Christensen U R, Theiβing J. 1995. The dynamics of plume-ridge interaction: 1. Ridge-centered plumes. Earth and Planetary Science Letters, 134(1-2): 155–168
Ruan Aiguo, Li Jiabiao, Niu Xiongwei, et al. 2014. Main characteristics of crustal structure of Southwest Indian Ridge. In: Committee of Information Technology, Chinese Geophysical Society. Abstract Set of Theses on Discussion and Application of Big Data, Cloud Computing and Geophysics (in Chinese). Shijiazhuang: Committee of Information Technology, Chinese Geophysical Society, 32–33
Sauter D, Cannat M. 2010. The ultraslow spreading Southwest Indian Ridge. In: Rona P A, Devey C W, Dyment J, et al., eds. Diversity of Hydrothermal Systems on Slow Spreading Ocean Ridges, Vol 88. Washington DC: American Geophysical Union, 153–173
Sauter D, Cannat M, Meyzen C, et al. 2009. Propagation of a melting anomaly along the ultraslow Southwest Indian Ridge between 46°E and 52°20′E: interaction with the Crozet hotspot. Geophysical Journal International, 179(2): 687–699
Sauter D, Mendel V, Rommevaux-Jestin C, et al. 2004. Focused magmatism versus amagmatic spreading along the ultra-slow

spreading Southwest Indian Ridge: Evidence from TOBI side scan sonar imagery. Geochemistry, Geophysics, Geosystems, 5(10): Q10K09

Sauter D, Patriat P, Rommevaux-Jestin C, et al. 2001. The Southwest Indian Ridge between 49°15′E and 57°E: focused accretion and magma redistribution. Earth and Planetary Science Letters, 192(3): 303–317

Seyler M, Cannat M, Mével C. 2003. Evidence for major-element heterogeneity in the mantle source of abyssal peridotites from the Southwest Indian Ridge (52° to 68°E). Geochemistry, Geophysics, Geosystems, 4(2): 9101

Standish J J, Dick H J B, Michael P J, et al. 2008. MORB generation beneath the ultraslow spreading Southwest Indian Ridge (9°–25°E): major element chemistry and the importance of process versus source. Geochemistry, Geophysics, Geosystems, 9(5): Q05004

Standish J J, Sims K W W. 2010. Young off-axis volcanism along the ultraslow-spreading Southwest Indian Ridge. Nature Geoscience, 3(4): 286–292

Stein C A, Stein S. 1994. Constraints on hydrothermal heat flux through the oceanic lithosphere from the global heat flow. Journal of Geophysical Research, 99(B2): 3081–3195

Suo Yanhui. 2014. Tectonic-magmatic processes of the Indian Ocean: evidence on the residual mantle Bouguer gravity anomaly (in Chinese) [dissertation]. Qingdao: Ocean University of China

Tao Chunhui, Li Huaiming, Jin Xiaobing, et al. 2014. Seafloor hydrothermal activity and polymetallic sulfide exploration on the southwest Indian ridge. Chinese Science Bulletin, 59(19): 2266–2276

Tao Chunhui, Lin Jian, Guo Shiqin, et al. 2012. First active hydrothermal vents on an ultraslow-spreading center: southwest Indian ridge. Geology, 40(1): 47–50

Tao Chunhui, Wu Tao, Jin Xiaobing, et al. 2013. Petrophysical characteristics of rocks and sulfides from the SWIR hydrothermal field. Acta Oceanologica Sinica, 32(12): 118–125

Tao Chunhui, Wu Guanghai, Ni Jianyu, et al. 2009. New hydrothermal fields found along the SWIR during the legs 5-7 of the Chinese DY115-20 Expedition. In: American Geophysical Union, Fall Meeting, Abstract OS21A-1150. Washington DC: American Geophysical Union

Tivey M K. 2007. Generation of seafloor hydrothermal vent fluids and associated mineral deposits. Oceanography, 20(1): 50–65

Tivey M A, Dyment J. 2010. The magnetic signature of hydrothermal systems in slow spreading environments. In: Rona P A, Devey C W, Dyment J, et al., eds. Diversity of Hydrothermal Systems on Slow Spreading Ocean Ridges. Washington DC: American Geophysical Union, 43–66

Tucholke B E, Lin Jian, Kleinrock M C. 1998. Megamullions and mullion structure defining oceanic metamorphic core complexes on the Mid-Atlantic Ridge. Journal of Geophysical Research, 103(B5): 9857–9866

Vine F J, Moores E M. 1972. A model for the gross structure, petrology, and magnetic properties of oceanic crust. Geological Society of America Memoirs, 132: 195–206

Yao Huiqiang, Tao Chunhui, Song Chengbing, et al. 2011. Integration study on mode for seafloor plolymetallic sulfide exploration. Journal of Central South University: Science and Technology (in Chinese), 42(S2): 114–122

Zhang Tao, Gao Jinyao, Chen Mei. 2005. The reasonable correction of eötvös effect in marine gravity survey. Hydrographic Surveying and Charting, 25(2): 17–20

Zhang Tao, Lin Jian, Gao Jinyao. 2011. Interactions between hotspots and the Southwest Indian Ridge during the last 90 Ma: implications on the formation of oceanic plateaus and intra-plate seamounts. Science China: Earth Sciences, 54(8): 1177–1188

Zhang Tao, Lin Jian, Gao Jinyao. 2013. Magmatism and tectonic processes in Area A hydrothermal vent on the Southwest Indian Ridge. Science China: Earth Sciences, 56(12): 2186–2197

Zhao Minghui, Qiu Xuelin, Li Jiabiao, et al. 2013. Three-dimensional seismic structure of the Dragon Flag oceanic core complex at the ultraslow spreading Southwest Indian Ridge (49°39′E). Geochemistry, Geophysics, Geosystems, 14(10): 4544–4563

Zhou Huaiyang, Dick H J B. 2013. Thin crust as evidence for depleted mantle supporting the Marion Rise. Nature, 494(7436): 195–200